

DSFormer: A Dual-domain Self-supervised Transformer for Accelerated Multi-contrast MRI Reconstruction

Bo Zhou^{1,2}, Jo Schlemper², Neel Dey^{2,3}, Seyed Sadegh Mohseni Salehi²,
Chi Liu¹, James S. Duncan¹, Michal Sofka²

¹Yale University

²Hyperfine Research

³New York University

Abstract

Multi-contrast MRI (MC-MRI) captures multiple complementary imaging modalities to aid in radiological decision-making. Given the need for lowering the time cost of multiple acquisitions, current deep accelerated MRI reconstruction networks focus on exploiting the redundancy between multiple contrasts. However, existing works are largely supervised with paired data and/or prohibitively expensive fully-sampled MRI sequences. Further, reconstruction networks typically rely on convolutional architectures which are limited in their capacity to model long-range interactions and may lead to suboptimal recovery of fine anatomical detail. To these ends, we present a dual-domain self-supervised transformer (DSFormer) for accelerated MC-MRI reconstruction. DSFormer develops a deep conditional cascade transformer (DCCT) consisting of several cascaded Swin transformer reconstruction networks (SwinRN) trained under two deep conditioning strategies to enable MC-MRI information sharing. We further present a dual-domain (image and k-space) self-supervised learning strategy for DCCT to alleviate the costs of acquiring fully sampled training data. DSFormer generates high-fidelity reconstructions which experimentally outperform current fully-supervised baselines. Moreover, we find that DSFormer achieves nearly the same performance when trained either with full supervision or with our proposed dual-domain self-supervision.

1. Introduction

Diagnosticians often capture a series of multi-contrast magnetic resonance images (MC-MRI) of a single subject to acquire complementary tissue information towards more accurate and comprehensive radiological evaluation [3, 23]. However, due to physical constraints, MRI intrinsically requires prolonged acquisition which often leads to patient discomfort and the accumulation of motion artifacts and system imperfections in the image that obfusc-

ate biomedically-relevant anatomical detail. These limitations have led to immense interest in accelerated methods that can reconstruct high-fidelity and artifact-free images from fewer (undersampled) frequency-domain (*k*-space) MRI measurements and reduced scan time.

While the inverse Fourier transform can reconstruct images from fewer *k*-space measurements, it comes at the cost of strong aliasing and blurring effects in the reconstruction and has thus motivated works which exploit transform-domain data priors to achieve higher quality reconstructions with fewer artifacts [8, 22, 25]. However, these methods may still yield blurred and sub-clinical reconstructions and are generally slow and hyperparameter-sensitive as they are based on iterative *instance-specific* optimization. More recently, deep MRI reconstruction networks [1, 5, 9, 11, 12, 19, 26, 27, 29, 30, 30, 33, 34, 36, 38–42] have greatly improved MRI reconstruction fidelity under high undersampling rates with prediction times on the order of seconds.

However, these works typically achieve their strong results via supervised training on ground-truth *fully sampled* images and/or *k*-space target data, which is often practically infeasible to acquire. Recently, a few *self-supervised* reconstruction frameworks have emerged requiring only undersampled *k*-space data [33, 38], yet their performance remains upper-bounded by full supervision. Further, whether supervised or self-supervised, the aforementioned works largely focus on single contrast MRI acceleration, whereas most diagnostics require MC-MRI. In MC-MRI reconstruction, fully sampled MRI modalities requiring shorter acquisitions can be used as a reference to guide target MRI modalities that require longer acquisitions via methods which inject a fully-sampled reference modality as an extra input channel into a reconstruction network [7, 18, 20, 31, 37, 41].

While these MC-MRI methods achieve excellent reconstructions, they have the following major limitations. First, previous MC-MRI reconstruction methods operate directly on the undersampled target MRI image as input (reconstructed via zero-padding and the inverse Fourier transform) and thus suffer from severe aliasing in their starting point.

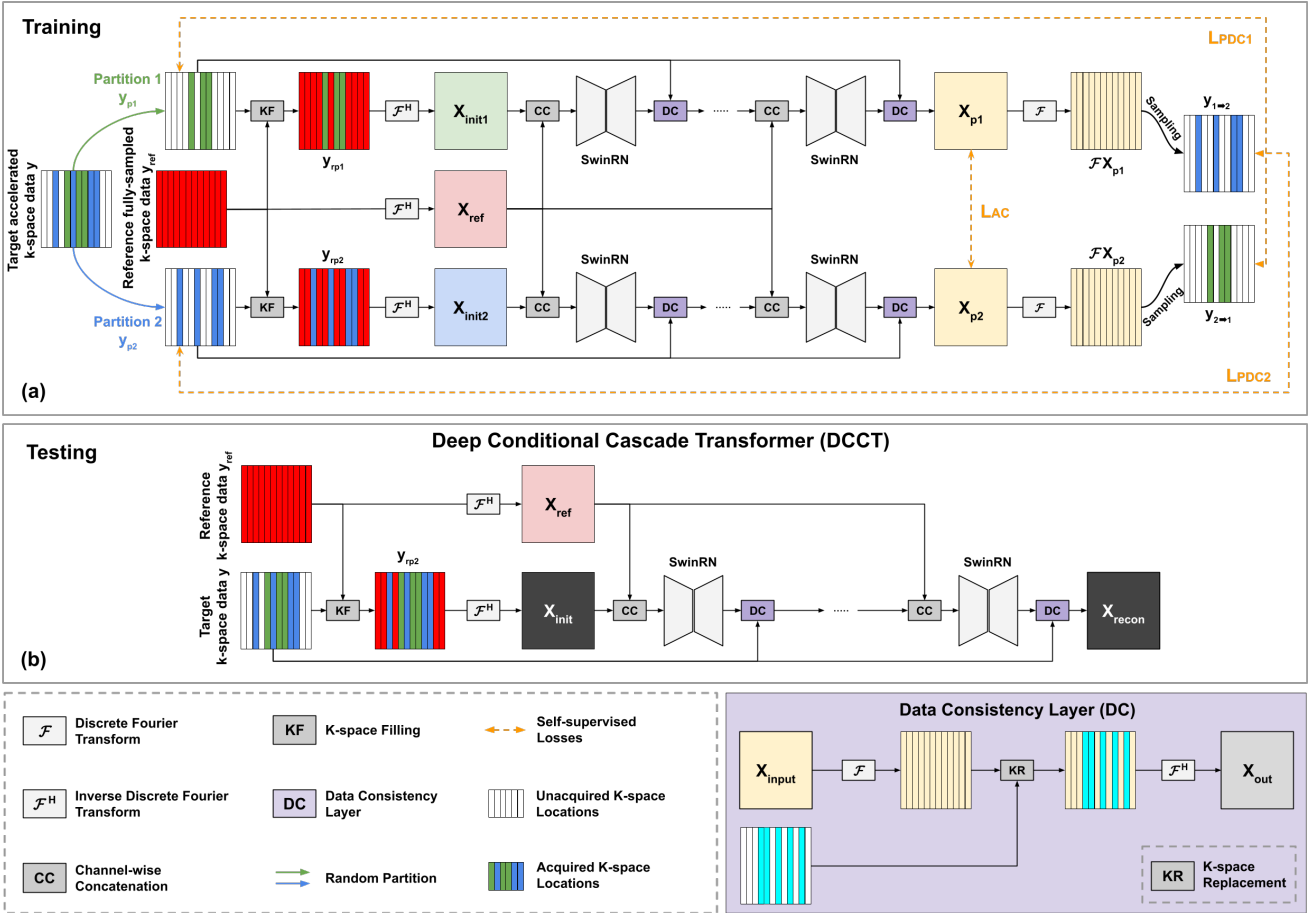


Figure 1. An overview of the **Dual-domain Self-supervised TransFormer (DSFormer)**. During training, a Deep Conditional Cascade Transformer (DCCT) is trained in a self-supervised fashion with randomly partitioned undersampled k-space data sets fed into DCCT in parallel. The partition data consistency loss (\mathcal{L}_{PDC}) and appearance consistency loss (\mathcal{L}_{AC}) are used for self-supervised training. At testing, arbitrarily undersampled data is reconstructed by DCCT. SwinRN (Fig. 3) is used as the backbone network for DCCT.

Second, current MC-MRI reconstruction networks ubiquitously employ convolutional architectures [7, 18, 28, 37], such as U-shape network designs [28], which are limited in modeling long-range interactions and may recover reduced fine image detail. Third, existing MC-MRI reconstruction methods require fully-supervised and fully-sampled training data from large-scale paired data, which is prohibitively expensive to obtain. The fully-sampled data of target contrasts demanding long acquisitions are also prone to motion and accumulated errors, thus self-supervised learning based on undersampled data with short acquisitions would be more robust to adversarial factors, such as motion.

To these ends, we present DSFormer, a dual-domain self-supervised transformer for fast MC-MRI reconstruction, with the following contributions:

1. *Multi-contrast information sharing.* We develop a deep MC-MRI conditioning method for efficient us-

age of multi-contrast information in MC-MRI reconstruction. Briefly, it leverages fully-sampled reference MRI data by grafting its k-space data into the unacquired k-space bins of the undersampled/accelerated target modality, whose inversion provides a sharp and de-aliased starting point for our network to train on (Figure 2). To further reinforce reference MRI information in the undersampled reconstruction, we also channel-wise concatenate the reference MRI reconstruction alongside the network inputs.

2. *Vision Transformers for MRI reconstruction.* Inspired by recent advances in vision transformers demonstrating improved image restoration over CNNs [6, 17, 21, 35] by using non-local processing, we develop a Swin transformer Reconstruction Network (SwinRN) to be used as a backbone in our cascaded framework. By combining MC-MRI conditioning with cas-

caded SwinRNs, we propose a Deep Conditional Cascade Transformer (DCCT) for high-fidelity MRI reconstruction.

3. *Dual-domain self-supervised learning.* To train DCCT in a self-supervised fashion using only undersampled target MRI data, we further propose a dual image and k-space domain self-supervised learning approach for DCCT training, achieving reconstruction quality comparable to fully supervised learning.

Extensive experiments on MC-MRI data with different acceleration protocols demonstrate that DSFormer trained with only self-supervision generates superior reconstructions over previous architectures and conditioning mechanisms with fully supervised training strategies. Finally, DCCT trained with dual-domain self-supervision achieves comparable performance to training under full-supervision.

2. Related work

Fully-supervised MRI reconstruction. Convolutional neural networks (CNNs) have been extensively studied to reconstruct images from undersampled k-space data. For example, Wang *et al.* [34] recover fully-sampled MRIs from undersampled acquisitions using supervised CNN training on paired data. Schlemper *et al.* [27, 29] develop a deep cascade of CNNs with intermediate data consistency layers which ensure that the originally-sampled k-space in the input is consistent with the reconstruction. Hammernik *et al.* [12] develop variational networks to solve reconstruction optimization using gradient descent with CNNs. Similarly, Aggarwal *et al.* [1] use a conjugate gradient algorithm within the reconstruction network.

In addition to methods operating in the image domain, dual image and k-space methods have also been explored. Eo *et al.* [9] add an additional k-space reconstruction network to [29] to enable cross-domain MRI reconstruction. Similarly, Singh *et al.* [30] show that combining frequency and image feature representation learning using two-task-independent layers can improve reconstruction performance over single-domain methods. Zhu *et al.* [42] directly map the undersampled k-space data to its image reconstruction using manifold learning. Moreover, reinforcement learning-aided reconstruction networks were also found to improve the reconstruction quality [26, 36]. While achieving promising performance, these methods typically require fully supervised training data from large-scale paired undersampled and fully sampled k-space scans [5, 16, 39].

Self-supervised MRI reconstruction. There are a handful of self-supervised MRI reconstruction methods that require only undersampled k-space data. HQS-Net [33] decouples the minimization of the data consistency term

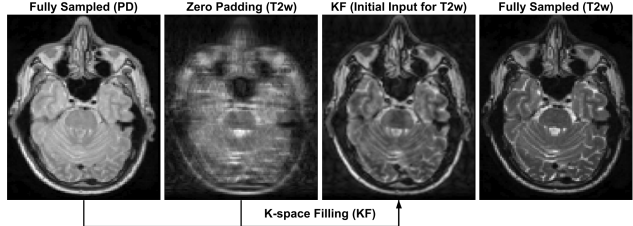


Figure 2. K-space filling (KF) conditioning for $\times 4$ accelerated T2w reconstruction. Undersampled T2w data is combined with fully sampled PD data via KF to generate an initial DCCT input generating much fewer artifacts as compared to zero-padding.

and regularization term in [29] based on a neural network, such that the deep network training relies only on undersampled measurements. Further, Yaman *et al.* [38] proposed a physically-guided self-supervised learning method that trains a reconstruction network by predicting one undersampled k-space data partition using the other data partition.

MC-MRI reconstruction. Currently, there are only a few deep learning-based fast MC-MRI reconstruction methods [7, 18, 20, 31, 37, 41]. Xiang *et al.* [37] use fully sampled T1w images as an additional CNN channel input to facilitate accelerated T2w reconstructions. Similarly, Dar *et al.* [7] add adversarial learning and a perceptual loss [14] to further improve performance. More recently, Liu *et al.* [18] and Zhou *et al.* [41] feed the fully sampled reference data as an additional channel input into a deep cascade network [29]. Similar strategies have also been proposed for variational MRI reconstruction training [12, 20].

3. Methods

The overall DSFormer pipeline is illustrated in Figure 1 and consists of two major parts: (1) the deep conditional cascade transformer reconstruction network architecture (Fig. 1b) and (2) the dual-domain self-supervised learning strategy used for training DCCT (Fig. 1a).

3.1. Deep Conditional Cascade Transformer

DCCT uses a cascaded network design with interleaved data consistency (DC) layers [24, 29]. To efficiently exploit multi-contrast information for reconstruction learning, we develop two deep multi-contrast network conditioning mechanisms to better leverage fully-sampled reference acquisitions. To further enable high-quality reconstruction, we propose a Swin Transformer Reconstruction Network (SwinRN) as the backbone network in DCCT.

Deep MC-MRI Conditioning. With MC-MRI, we use two conditioning methods for sharing reference MRI with tar-

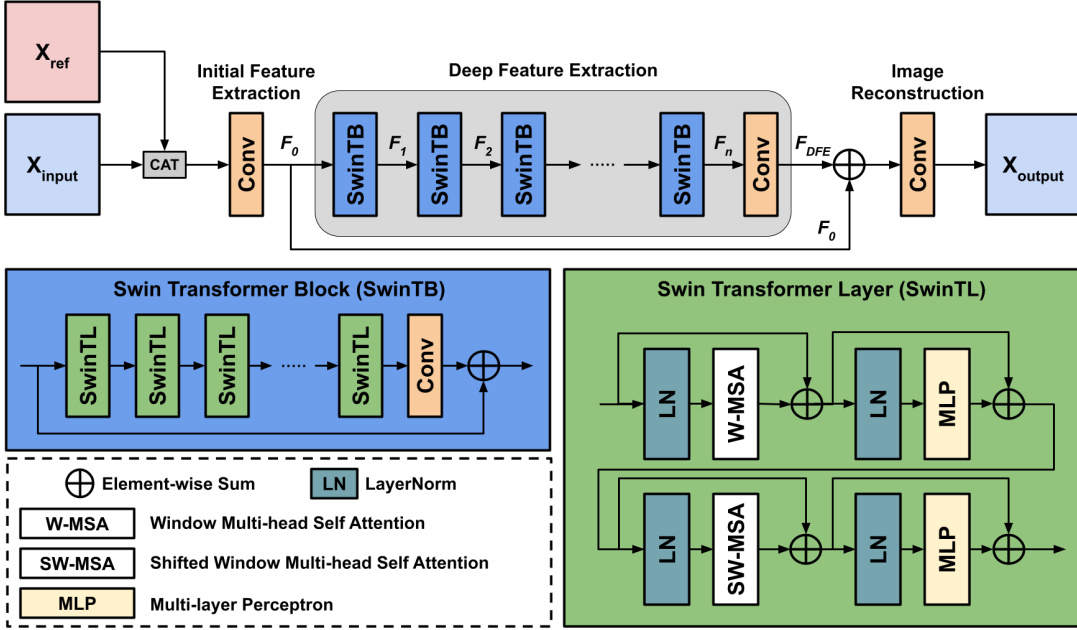


Figure 3. The architecture of Swin Transformer Reconstruction Network (SwinRN). It consists of initial feature extraction, deep feature extraction, and image reconstruction modules, and is used as the backbone reconstruction network in Figure 1.

get MRI in DCCT: K-space Filling (KF) conditioning and Channel-wise (CC) conditioning. First, we use KF, because multi-contrast MRI depicts distinct physiological properties of imaged tissues, resulting in different image contrast, but the multi-contrast MRI images share the same anatomy. While target contrast zero-padded reconstruction with undersampled k-space data could result in severe artifacts, filling the unacquired k-space with reference contrast k-space data (assuming no motion between the target and reference) can produce alias-reduced reconstruction with the same anatomy and altered contrast. This KF reconstruction can be used as initial DCCT input, so that it can focus on learning contrast conversion instead of de-aliasing. An example of KF is shown in Fig. 2.

In addition to KF, we also use CC. As illustrated in Figure 1b, the first input to the cascade is the channel-wise concatenation of KF target and the reference contrast MRI image, while the following cascade inputs are the channel-wise concatenations of the previous cascade output and the reference contrast MRI image.

Swin Transformer Reconstruction Network. SwinRN is used as the backbone network for DCCT with its architecture shown in Figure 3. SwinRN consists of three modules: initial feature extraction (IFE) using a 3×3 convolutional layer, deep feature extraction (DFE) using multiple Swin Transformer Blocks (SwinTB), and image reconstruction using global residual learning and a 3×3 convolution

layer. The workflow is as follows,

$$F_0 = P_{IFE}(X_{init} | X_{ref}), \quad (1)$$

where P_{IFE} denotes the IFE operation and $| \cdot$ denotes conditional input. The IFE feature F_0 is then used for residual learning in the reconstruction step and is fed into multiple SwinTBs for DFE. If there are n SwinTBs, the n -th output F_n is

$$F_n = P_{SwinTB_n}(F_{n-1}). \quad (2)$$

Then, the output of DFE is given by $F_{DFE} = P_{DFE}(F_n)$, where P_{DFE} is a 3×3 convolutional layer for final feature fusion in DFE. Given F_{DFE} and the global residual connection of F_{IFE} , the final reconstruction can be generated via

$$X_{output} = P_{IR}(F_{DFE} + F_{IFE}), \quad (3)$$

where P_{IR} is another 3×3 convolutional layer for generating a one-channel image reconstruction output.

Swin Transformer Block. Each SwinTB (Fig. 3) consists of multiple Swin transformer layers (SwinTL), a convolution layer for local feature fusion, and a residual connection for local residual learning. Given the input feature $F_{i,0}$ of the i -th SwinTB, the intermediate feature is written as:

$$F_{i,j} = P_{SwinTL_{i,j}}(F_{i,j-1}), \quad (4)$$

where $P_{SwinTL_{i,j}}(\cdot)$ is the j -th SwinTL in the i -th SwinTB. Then, local feature fusion and local residual learning is applied to generate the SwinTB output:

$$F_i = P_{LFF_i}(F_{i,K}) + F_{i,0}, \quad (5)$$

where K is the number of SwinTL in SwinTB and P_{LFF_i} is a convolutional layer for SwinTB's i -th local feature fusion.

SwinTL [21] consists of layer normalization (LN), multi-layer perceptrons (MLP), and multi-head self attention (MSA) modules [32] with regular windowing (W-MSA) and shifted windowing (SW-MSA) configurations. Given a input with feature size $H \times W \times C$, SwinTL first reshapes the input into $(M \times M) \times (\frac{H}{M} \times \frac{W}{M}) \times C$ by partitioning it into non-overlapping $\frac{H}{M} \times \frac{W}{M}$ windows with each window containing $M \times M$ patches. Then, self-attention can be computed for each window [32] and can formulate the attention output of W-MSA. To enable cross-window connection, self-attention is also computed for each window by shifting the feature by $(\lfloor \frac{M}{2} \rfloor, \lfloor \frac{M}{2} \rfloor)$ before partitioning. SwinTL processing (Fig. 3) can thus be summarized as,

$$\bar{z} = W\text{-MSA}(LN(z)) + z, \quad (6)$$

$$\ddot{z} = MLP(LN(\bar{z})) + \bar{z}, \quad (7)$$

$$\hat{z} = SW\text{-MSA}(LN(\ddot{z})) + \ddot{z}, \quad (8)$$

$$\check{z} = MLP(LN(\hat{z})) + \hat{z}, \quad (9)$$

where MLP is a 2-layer MLP with a GELU activation [13].

In summary, SwinRN with basic blocks of SwinTB is embedded in the cascaded framework of DCCT for MRI reconstruction. We use a 3-cascade of SwinRNs with each SwinRN sharing the same parameters. The number of SwinTB in each SwinRN is set to 4 with each SwinTB containing 4 SwinTL.

3.2. Dual-Domain Self-Supervised Learning

To train DCCT in a self-supervised fashion without using any fully-sampled ground truth data in the target domain, we propose dual-domain self-supervision, as illustrated in Figure 1. Let $f_{dcct}(y_{tag}, y_{ref})$ denote DCCT, where y_{tag} is the target contrast's undersampled data and y_{ref} is the reference contrast's fully sampled data. During training, we first randomly partition y_{tag} into two disjoint sets via,

$$y_{p1} = y_{tag} \odot M_1 \text{ and } y_{p2} = y_{tag} \odot M_2, \quad (10)$$

where \odot is element-wise multiplication. M_1 and M_2 are binary k-space masks for partition 1 and partition 2. Note that $M_1 + M_2 = M_{tag}$, where M_{tag} is the binary mask indicating all under-sampled locations. The partitions y_{p1} and y_{p2} are then fed into DCCT for parallel reconstruction,

$$X_{p1} = f_{dcct}(y_{p1}, y_{ref}) \text{ and } X_{p2} = f_{dcct}(y_{p2}, y_{ref}), \quad (11)$$

where the networks share the same parameters. The reconstructions of y_{p1} and y_{p2} should be consistent with each other. Thus, our first loss is an Appearance Consistency (AC) loss operating in the image domain as,

$$\mathcal{L}_{AC} = \lambda_1 \mathcal{L}_{img} + \lambda_2 \mathcal{L}_{grad}, \quad (12)$$

$$\text{where } \mathcal{L}_{img} = \|X_{p1} - X_{p2}\|_1 \text{ and,} \quad (13)$$

$$\begin{aligned} \mathcal{L}_{grad} = & \|\nabla_v X_{p1} - \nabla_v X_{p2}\|_1 \\ & + \|\nabla_h X_{p1} - \nabla_h X_{p2}\|_1, \end{aligned} \quad (14)$$

where ∇_v and ∇_h are vertical and horizontal intensity gradient operators, respectively. We set $\lambda_1 = 1$ and $\lambda_2 = 0.1$.

Our second loss corresponds to a Partition Data Consistency (PDC) loss which operates in k-space. If DCCT can generate a high-quality image from any undersampled k-space measurement, the k-space data of the image predicted from the first partition y_{p1} should be consistent with the other partition y_{p2} and vice versa. The predicted k-space partition can be written as,

$$y_{2 \rightarrow 1} = \mathcal{F}(X_{p2}) \odot M_1 \text{ and } y_{1 \rightarrow 2} = \mathcal{F}(X_{p1}) \odot M_2, \quad (15)$$

Therefore, the PDC loss is formulated as,

$$\mathcal{L}_{PDC} = \|y_{2 \rightarrow 1} - y_{p1}\|_1 + \|y_{1 \rightarrow 2} - y_{p2}\|_1, \quad (16)$$

where the first and second term are the data consistency losses for partitions 1 and 2, respectively. Combining the AC loss in the image domain and the PDC loss in k-space, our total loss can be written as,

$$\mathcal{L}_{tot} = \mathcal{L}_{AC} + \lambda_3 \mathcal{L}_{PDC} \quad (17)$$

where $\lambda_3 = 0.1$ is used to balance the scale between k-space and image domain losses.

4. Experiments

4.1. Experimental Settings

Data and Training. We use 578 MC-MRI subjects with both T2-weighted and Proton Density (PD)-weighted acquisitions from IXI¹ for our experiments. The registered MC-MRI data consisting of 11808 pairs of T2 and PD weighted axial slices were split subject-wise into 8376 pairs for training, 1080 for validation, and 2352 for testing, with no slices from any subject overlapping. We consider two MC-MRI scenarios in our experiments: accelerating T2-weighted acquisition (the target protocol) by utilizing a fully sampled PD-weighted acquisition (reference protocol), and accelerating PD-weighted target acquisition with a fully sampled T2-weighted reference. Here, we consider the Cartesian sampling pattern with the acceleration factor (R) set to a

¹<https://brain-development.org/ixi-dataset/>, CC BY-SA 3.0 license

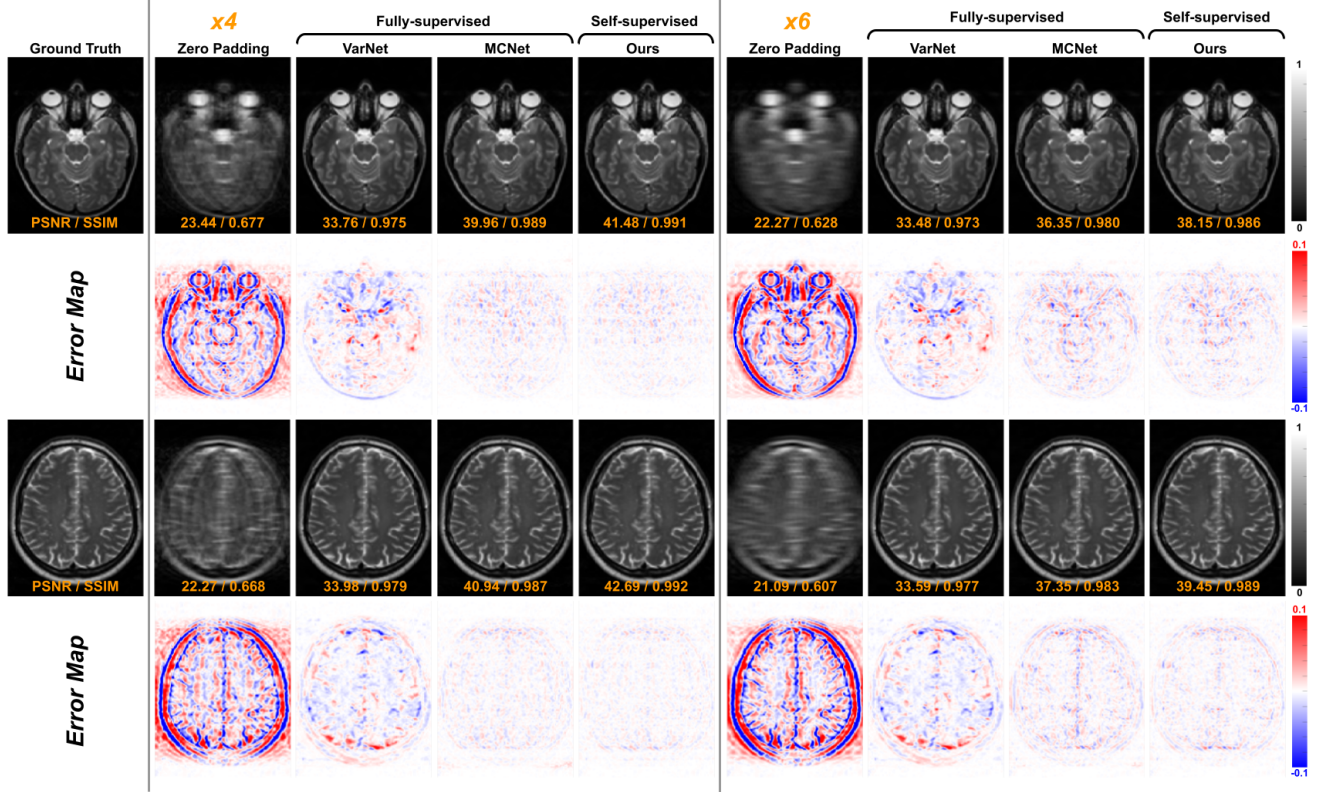


Figure 4. Qualitative comparisons of T2 reconstructions using $\times 4$ and $\times 6$ accelerations. For T2 reconstruction, PD is used as the reference contrast. The corresponding error maps between ground truth images and the reconstructions are illustrated in the 2nd and 4th rows

Table 1. Quantitative comparison of T2 (left sub-table) and PD (right sub-table) reconstructions under three different acceleration settings for the target contrast MRI. Best results are marked in red. The number of parameters used in the network is indicated in the last column.

PSNR/SSIM Methods	Target: T2w Reference: PD			Target: PD Reference: T2w			Number of Parameters
	$\times 2$	$\times 4$	$\times 6$	$\times 2$	$\times 4$	$\times 6$	
Zero-padding	24.86/0.761	22.72/0.679	21.48/0.623	23.92/0.744	21.68/0.663	20.47/0.610	-
UFNet [37]	32.30/0.970	32.07/0.969	31.85/0.967	32.22/0.971	32.06/0.969	31.88/0.968	7.6M
VarNet [20]	33.01/0.973	32.71/0.971	32.43/0.970	33.08/0.974	32.86/0.972	32.67/0.970	8.2M
MCNet [18]	43.79/0.989	39.14/0.983	35.61/0.972	42.90/0.988	38.56/0.979	35.45/0.971	0.11M
DSFormer	45.05/0.993	40.31/0.985	37.04/0.977	45.07/0.993	40.52/0.987	37.45/0.982	0.18M

value between 2 and 8 corresponding to acceleration in acquisition time for the target protocol.

We implement all methods in Pytorch and perform experiments using an NVIDIA Quadro RTX 8000 GPU with 48GB memory. The Adam solver [15] was used to optimize our models with $lr = 2 \times 10^{-4}$, $\beta_1 = 0.9$, and $\beta_2 = 0.999$. We use a batch size of 3 during training. In DSFormer, the default number of cascade is set to 3 with each cascading SwinRN shares the same parameters. The number of SwinTB in each SwinRN is set to 4 with each SwinTB containing 4 SwinTL. During training, the undersampled data partitioning rate is randomly generated between [0.2, 0.8].

Baselines and Evaluation. Benchmark results are presented on 2352 test slices from 114 patients. We eval-

uate the target reconstruction results using Peak Signal-to-Noise Ratio (PSNR) and Structural Similarity Index (SSIM) computed against ground truth and compare our results against fully-supervised methods that require ground truth fully-sampled data, including UFNet [37], MCNet [18], and VarNet [20]. As an upper bound, we also compare self-supervised DSFormer against a supervised-strategy where the DCCT of DSFormer was trained in a fully supervised fashion with ground truth available.

4.2. Results

Image Quality Evaluation and Comparison. Quantitative evaluations on two different MC-MRI scenarios under three different acceleration settings are summarized in Ta-

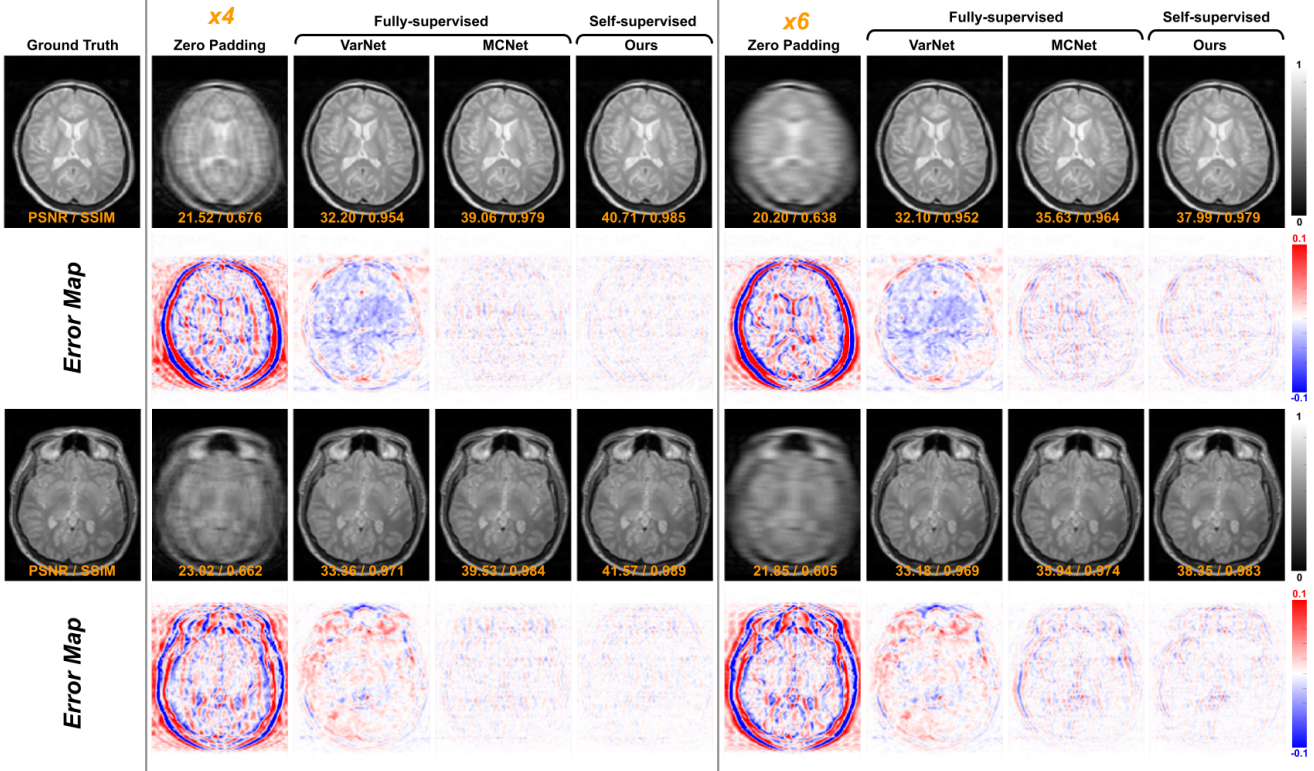


Figure 5. Qualitative comparisons of PD reconstructions using $\times 4$ and $\times 6$ accelerations. For PD reconstruction, T2 is used as the reference contrast. The corresponding reconstruction error maps are illustrated in the 2nd and 4th rows, calculated between ground truth and the network reconstructions.

ble 1. The left sub-table summarizes MC-MRI reconstruction with T2 target contrast and PD reference contrast (T2 reconstructions were evaluated here). Among fully supervised methods, MCNet [18] achieves the best T2 reconstruction performance with PSNR up to 43.79 dB and SSIM up to 0.989 when using $\times 2$ acceleration. DSFormer trained with self-supervision alone outperforms supervised baselines and increases PSNR from 43.79 dB to 45.05 dB and SSIM from 0.989 to 0.993. Similar observations are made for the $\times 4$ accelerated T2 experiments where DSFormer outperformed MCNet, with PSNR increasing from 39.14 dB to 40.31 dB and SSIM increasing from 0.983 to 0.985. As expected, the reconstruction performance of all methods decreases as the acceleration rate increases. However, DSFormer is still able to widely outperform previous supervised methods and keep PSNR at 37.04 and SSIM at 0.977 with $\times 6$ accelerated T2 reconstruction.

The qualitative comparison of various T2 reconstructions is shown in Fig. 4, illustrating $\times 4$ and $\times 6$ acceleration settings. Reconstructions with zero padding create significant aliasing artifacts and lose anatomical details. While both VarNet [20] and MCNet [18] significantly reduce the aliasing artifacts with decreased reconstruction error, they

Table 2. Quantitative comparison of T2 reconstruction performance from different self-supervision settings, including image-domain only self-supervision, k-space only self-supervision, and the proposed dual-domain self-supervision. Higher is better.

PSNR/SSIM	$\times 2$	$\times 4$
Only k-space self-supervision	44.69/0.991	40.23/0.982
Only image self-supervision	43.86/0.990	39.95/0.981
Ours	45.05/0.993	40.31/0.985

require fully supervised training from paired data. On the other hand, DSFormer, using only self-supervision, further reduces the residual error between the reconstruction and the ground truth, generating superior reconstruction quality.

The right sub-table of Table 1 summarizes MC-MRI with PD target contrast and T2 reference contrast, where PD reconstructions were evaluated. Similar observations are made for PD reconstruction, where DSFormer still achieves the best reconstruction under all three acceleration settings over previous fully supervised methods [18, 20, 37]. The qualitative comparison of several PD reconstruction methods is shown in Fig. 5, highlighting $\times 4$ and $\times 6$ acceleration settings. Qualitatively, DSFormer produces the best reconstruction with the least residual error.

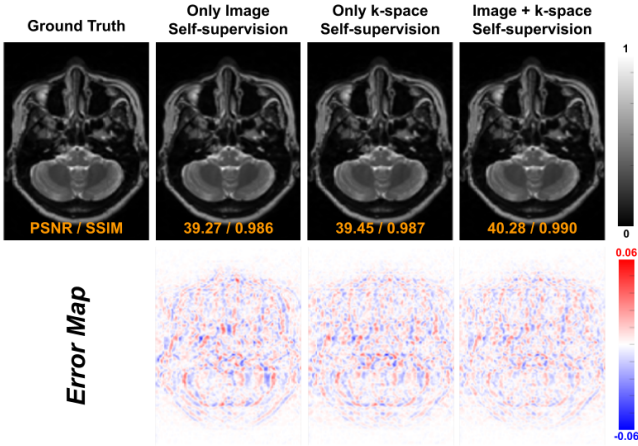


Figure 6. Visual comparisons of MRI reconstruction from different self-supervision settings. Lower residual error is better. T2 reconstruction and $\times 4$ acceleration is considered here.

4.3. Ablation Studies

Dual-domain self-supervision. To isolate the individual utility of the various components of dual-domain self-supervision, we evaluate reconstruction performance using either only image-domain self-supervision (\mathcal{L}_{AC}) or only k-space self-supervision (\mathcal{L}_{PDC}). The quantitative comparison is summarized in Table 2. We observe that using either only k-space self-supervision or only image-domain self-supervision still yields strong reconstruction quality, with a PSNR of 39.95 under $\times 4$ acceleration, which indicates self-supervision in both domains can help with reconstruction. Importantly, DSFormer with only image-domain self-supervision or only k-space self-supervision still outperforms all previous fully supervised methods (Table 1). As expected, combining both image-domain and k-space self-supervision yields the best reconstruction performance. A visual comparison of reconstructions from different self-supervision settings is illustrated in Figure 6. Similar to observations made in Table 2, DSFormer with dual-domain self-supervision has the least residual error as compared to single domain self-supervision.

Deep MC-MRI conditioning. To understand the impact of KF as the initial network input, we evaluate DSFormer reconstruction performance with or without KF, with quantification summarized in Table 3. Under $\times 4$ acceleration, DSFormer without KF can already generate high-quality reconstructions with 40.22 dB PSNR and using KF further improves performance to 40.31 dB PSNR, with similar trends observed in the $\times 2$ experiments.

Fully-supervised vs. Self-supervised DSFormer. As DSFormer is self-supervised with no paired data used in train-

Table 3. Quantitative comparison of T2 reconstruction performance when using DSFormer with or without KF and when training DSFormer in a fully supervised manner similar to [18, 37] without our proposed consistency losses.

PSNR/SSIM	$\times 2$	$\times 4$
Ours w/o KF	44.88/0.991	40.22/0.982
Ours	45.05/0.993	40.31/0.985
Supervised (Upper Bound)	45.06/0.994	40.34/0.989

ing, in order to understand the performance gap between full supervision and our dual-domain self-supervision, we also compare the reconstruction performance of DCCT trained without partitioning the input and replacing its consistency losses with direct image-domain reconstruction losses against the target ground truth, same as the supervised training in [18, 37]. The quantitative comparison is summarized in Table 3. As an upper bound, the fully supervised DSFormer achieved reconstruction PSNR of 40.34 dB under $\times 4$ acceleration, which is only ~ 0.03 higher than self-supervised DSFormer in terms of PSNR.

5. Discussion and Conclusion

Limitations and future work. The presented work has limitations with several potential improvements that are the subjects of our future work. First, dual-domain self-supervision requires an accurate k-space signal for loss computation. Increased noise in undersampled data may impact training performance, and thus pre-processing via denoising could be applied to stabilize the self-supervised training. Second, the proposed conditioning method requires well-aligned MC-MRI. As misalignment between MC-MRI may degrade DSFormer performance, image registration should be considered in the pre-processing to eliminate the effect [2, 4, 10]. Third, currently, DSFormer only considers accelerating the target MRI in MC-MRI, while acquiring fully sampled reference MRI. DSFormer could be extended to simultaneous accelerated MC-MRI for all contrasts, which is an important direction for future work. Importantly, our experiments benchmark DSFormer’s performance only on healthy human data and it is plausible that pathologies (e.g., lesions) may lead to drastically different appearances in some modality pairs. In future work, we will investigate reconstruction on pathological data with heterogeneous tissue appearance.

Conclusions. In this work, we develop DSFormer, a novel dual-domain self-supervised transformer for accelerated multi-contrast MRI reconstruction. DSFormer proposes a deep conditional cascaded transformer that is trained with k-space and image domain self-supervisions. Experimental benchmarks demonstrate the DSFormer outperforms previous *fully supervised methods* that require training with

paired data (Table 1) and that DSFormer achieves nearly the same performance when trained with either full supervision or with our proposed dual-domain self-supervision (Table 3), thus closing the gap between supervised and self-supervised methods for accelerated MRI reconstruction.

References

- [1] Hemant K Aggarwal, Merry P Mani, and Mathews Jacob. Modl: Model-based deep learning architecture for inverse problems. *IEEE transactions on medical imaging*, 38(2):394–405, 2018. [1](#) [3](#)
- [2] Brian B Avants, Nick Tustison, Gang Song, et al. Advanced normalization tools (ants). *Insight j*, 2(365):1–35, 2009. [8](#)
- [3] Spyridon Bakas, Hamed Akbari, Aristeidis Sotiras, Michel Bilello, Martin Rozycki, Justin S Kirby, John B Freymann, Keyvan Farahani, and Christos Davatzikos. Advancing the cancer genome atlas glioma mri collections with expert segmentation labels and radiomic features. *Scientific data*, 4(1):1–13, 2017. [1](#)
- [4] Guha Balakrishnan, Amy Zhao, Mert R Sabuncu, John Guttag, and Adrian V Dalca. Voxelmorph: a learning framework for deformable medical image registration. *IEEE transactions on medical imaging*, 38(8):1788–1800, 2019. [8](#)
- [5] Nicholas Bien, Pranav Rajpurkar, Robyn L Ball, Jeremy Irvin, Allison Park, Erik Jones, Michael Bereket, Bhavik N Patel, Kristen W Yeom, Katie Shpanskaya, et al. Deep-learning-assisted diagnosis for knee magnetic resonance imaging: development and retrospective validation of mrnet. *PLoS medicine*, 15(11):e1002699, 2018. [1](#) [3](#)
- [6] Hanting Chen, Yunhe Wang, Tianyu Guo, Chang Xu, Yiping Deng, Zhenhua Liu, Siwei Ma, Chunjing Xu, Chao Xu, and Wen Gao. Pre-trained image processing transformer. In *Proceedings of the IEEE/CVF Conference on Computer Vision and Pattern Recognition*, pages 12299–12310, 2021. [2](#)
- [7] Salman UH Dar, Mahmut Yurt, Mohammad Shahdloo, Muhammed Emrullah Ildiz, Berk Tinaz, and Tolga Çukur. Prior-guided image reconstruction for accelerated multi-contrast mri via generative adversarial networks. *IEEE Journal of Selected Topics in Signal Processing*, 14(6):1072–1087, 2020. [1](#) [2](#) [3](#)
- [8] David L Donoho, Arian Maleki, and Andrea Montanari. Message-passing algorithms for compressed sensing. *Proceedings of the National Academy of Sciences*, 106(45):18914–18919, 2009. [1](#)
- [9] Taejoon Eo, Yohan Jun, Taeseong Kim, Jinseong Jang, Ho-Joon Lee, and Dosik Hwang. Kiki-net: cross-domain convolutional neural networks for reconstructing undersampled magnetic resonance images. *Magnetic resonance in medicine*, 80(5):2188–2201, 2018. [1](#) [3](#)
- [10] Bruce Fischl. Freesurfer. *Neuroimage*, 62(2):774–781, 2012. [8](#)
- [11] Pengfei Guo, Jeya Maria Jose Valanarasu, Puyang Wang, Jinyuan Zhou, Shanshan Jiang, and Vishal M Patel. Over-and-under complete convolutional rnns for mri reconstruction. *arXiv preprint arXiv:2106.08886*, 2021. [1](#)
- [12] Kerstin Hammernik, Teresa Klatzer, Erich Kobler, Michael P Recht, Daniel K Sodickson, Thomas Pock, and Florian Knoll. Learning a variational network for reconstruction of accelerated mri data. *Magnetic resonance in medicine*, 79(6):3055–3071, 2018. [1](#) [3](#)
- [13] Dan Hendrycks and Kevin Gimpel. Gaussian error linear units (gelus). *arXiv preprint arXiv:1606.08415*, 2016. [5](#)
- [14] Justin Johnson, Alexandre Alahi, and Li Fei-Fei. Perceptual losses for real-time style transfer and super-resolution. In *European conference on computer vision*, pages 694–711. Springer, 2016. [3](#)
- [15] Diederik P Kingma and Jimmy Ba. Adam: A method for stochastic optimization. *arXiv preprint arXiv:1412.6980*, 2014. [6](#)
- [16] Florian Knoll, Jure Zbontar, Anuroop Sriram, Matthew J Muckley, Mary Bruno, Aaron Defazio, Marc Parente, Krzysztof J Geras, Joe Katsnelson, Hersh Chandarana, et al. fastmri: A publicly available raw k-space and dicom dataset of knee images for accelerated mr image reconstruction using machine learning. *Radiology: Artificial Intelligence*, 2(1):e190007, 2020. [3](#)
- [17] Jingyun Liang, Jiezhang Cao, Guolei Sun, Kai Zhang, Luc Van Gool, and Radu Timofte. Swinir: Image restoration using swin transformer. In *Proceedings of the IEEE/CVF International Conference on Computer Vision*, pages 1833–1844, 2021. [2](#)
- [18] Xinwen Liu, Jing Wang, Jin Jin, Mingyan Li, Fangfang Tang, Stuart Crozier, and Feng Liu. Deep unregistered multi-contrast mri reconstruction. *Magnetic Resonance Imaging*, 2021. [1](#) [2](#) [3](#) [6](#) [7](#) [8](#)
- [19] Xinwen Liu, Jing Wang, Feng Liu, and S Kevin Zhou. Universal undersampled mri reconstruction. *arXiv preprint arXiv:2103.05214*, 2021. [1](#)
- [20] Xinwen Liu, Jing Wang, Hongfu Sun, Shekhar S Chandra, Stuart Crozier, and Feng Liu. On the regularization of feature fusion and mapping for fast mr multi-contrast imaging via iterative networks. *Magnetic resonance imaging*, 77:159–168, 2021. [1](#) [3](#) [6](#) [7](#)
- [21] Ze Liu, Yutong Lin, Yue Cao, Han Hu, Yixuan Wei, Zheng Zhang, Stephen Lin, and Baining Guo. Swin transformer: Hierarchical vision transformer using shifted windows. *arXiv preprint arXiv:2103.14030*, 2021. [2](#) [5](#)
- [22] Michael Lustig, David Donoho, and John M Pauly. Sparse mri: The application of compressed sensing for rapid mr imaging. *Magnetic Resonance in Medicine: An Official Journal of the International Society for Magnetic Resonance in Medicine*, 58(6):1182–1195, 2007. [1](#)
- [23] Bjoern H Menze, Andras Jakab, Stefan Bauer, Jayashree Kalpathy-Cramer, Keyvan Farahani, Justin Kirby, Yuliya Burren, Nicole Porz, Johannes Slotboom, Roland Wiest, et al. The multimodal brain tumor image segmentation benchmark (brats). *IEEE transactions on medical imaging*, 34(10):1993–2024, 2014. [1](#)
- [24] Matthew J Muckley, Bruno Riemenschneider, Alireza Radmanesh, Sunwoo Kim, Geunu Jeong, Jingyu Ko, Yohan Jun, Hyungseob Shin, Dosik Hwang, Mahmoud Mostapha, et al. Results of the 2020 fastmri challenge for machine learning mr image reconstruction. *IEEE transactions on medical imaging*, 40(9):2306–2317, 2021. [3](#)

[25] Ricardo Otazo, Daniel Kim, Leon Axel, and Daniel K Sodickson. Combination of compressed sensing and parallel imaging for highly accelerated first-pass cardiac perfusion mri. *Magnetic resonance in medicine*, 64(3):767–776, 2010. [1](#)

[26] Luis Pineda, Sumana Basu, Adriana Romero, Roberto Calandra, and Michal Drodzal. Active mr k-space sampling with reinforcement learning. In *International Conference on Medical Image Computing and Computer-Assisted Intervention*, pages 23–33. Springer, 2020. [1, 3](#)

[27] Chen Qin, Jo Schlemper, Jose Caballero, Anthony N Price, Joseph V Hajnal, and Daniel Rueckert. Convolutional recurrent neural networks for dynamic mr image reconstruction. *IEEE transactions on medical imaging*, 38(1):280–290, 2018. [1, 3](#)

[28] Olaf Ronneberger, Philipp Fischer, and Thomas Brox. U-net: Convolutional networks for biomedical image segmentation. In *International Conference on Medical image computing and computer-assisted intervention*, pages 234–241. Springer, 2015. [2](#)

[29] Jo Schlemper, Jose Caballero, Joseph V Hajnal, Anthony N Price, and Daniel Rueckert. A deep cascade of convolutional neural networks for dynamic mr image reconstruction. *IEEE transactions on Medical Imaging*, 37(2):491–503, 2017. [1, 3](#)

[30] Nalini M Singh, Juan Eugenio Iglesias, Elfar Adalsteinsson, Adrian V Dalca, and Polina Golland. Joint frequency and image space learning for fourier imaging. *arXiv preprint arXiv:2007.01441*, 2020. [1, 3](#)

[31] Liyan Sun, Zhiwen Fan, Xueyang Fu, Yue Huang, Xinghao Ding, and John Paisley. A deep information sharing network for multi-contrast compressed sensing mri reconstruction. *IEEE Transactions on Image Processing*, 28(12):6141–6153, 2019. [1, 3](#)

[32] Ashish Vaswani, Noam Shazeer, Niki Parmar, Jakob Uszkoreit, Llion Jones, Aidan N Gomez, Łukasz Kaiser, and Illia Polosukhin. Attention is all you need. In *Advances in neural information processing systems*, pages 5998–6008, 2017. [5](#)

[33] Alan Q Wang, Adrian V Dalca, and Mert R Sabuncu. Neural network-based reconstruction in compressed sensing mri without fully-sampled training data. In *International Workshop on Machine Learning for Medical Image Reconstruction*, pages 27–37. Springer, 2020. [1, 3](#)

[34] Shanshan Wang, Zhenghang Su, Leslie Ying, Xi Peng, Shun Zhu, Feng Liang, Dagan Feng, and Dong Liang. Accelerating magnetic resonance imaging via deep learning. In *2016 IEEE 13th International Symposium on Biomedical Imaging (ISBI)*, pages 514–517. IEEE, 2016. [1, 3](#)

[35] Zhendong Wang, Xiaodong Cun, Jianmin Bao, and Jianzhuang Liu. Uformer: A general u-shaped transformer for image restoration. *arXiv preprint arXiv:2106.03106*, 2021. [2](#)

[36] Kaixuan Wei, Angelica Aviles-Rivero, Jingwei Liang, Ying Fu, Carola-Bibiane Schönlieb, and Hua Huang. Tuning-free plug-and-play proximal algorithm for inverse imaging problems. In *International Conference on Machine Learning*, pages 10158–10169. PMLR, 2020. [1, 3](#)

[37] Lei Xiang, Yong Chen, Weitang Chang, Yiqiang Zhan, Weili Lin, Qian Wang, and Dinggang Shen. Ultra-fast t2-weighted mr reconstruction using complementary t1-weighted information. In *International Conference on Medical Image Computing and Computer-Assisted Intervention*, pages 215–223. Springer, 2018. [1, 2, 3, 6, 7, 8](#)

[38] Burhaneddin Yaman, Seyed Amir Hosseini Hosseini, Steen Moeller, Jutta Ellermann, Kâmil Uğurbil, and Mehmet Akçakaya. Self-supervised learning of physics-guided reconstruction neural networks without fully sampled reference data. *Magnetic resonance in medicine*, 84(6):3172–3191, 2020. [1, 3](#)

[39] Jure Zbontar, Florian Knoll, Anuroop Sriram, Tullie Murrill, Zhengnan Huang, Matthew J Muckley, Aaron Defazio, Ruben Stern, Patricia Johnson, Mary Bruno, et al. fastmri: An open dataset and benchmarks for accelerated mri. *arXiv preprint arXiv:1811.08839*, 2018. [1, 3](#)

[40] Zizhao Zhang, Adriana Romero, Matthew J Muckley, Pascal Vincent, Lin Yang, and Michal Drodzal. Reducing uncertainty in undersampled mri reconstruction with active acquisition. In *Proceedings of the IEEE Conference on Computer Vision and Pattern Recognition*, pages 2049–2058, 2019. [1](#)

[41] Bo Zhou and S Kevin Zhou. Dudonet: Learning a dual-domain recurrent network for fast mri reconstruction with deep t1 prior. In *Proceedings of the IEEE/CVF Conference on Computer Vision and Pattern Recognition*, pages 4273–4282, 2020. [1, 3](#)

[42] Bo Zhu, Jeremiah Z Liu, Stephen F Cauley, Bruce R Rosen, and Matthew S Rosen. Image reconstruction by domain-transform manifold learning. *Nature*, 555(7697):487, 2018. [1, 3](#)